applied sciences

MDPI

Technical Note

The Effects of Tangential Ground–Lining Interaction on Segmental Lining Behavior Using the Beam-Spring Model

Anh The Pham [1,2,*] and Mitsutaka Sugimoto [1]

1 Department of Civil and Environmental Engineering, Nagaoka University of Technology, Nagaoka, Niigata 940-2188, Japan; sugimo@vos.nagaokaut.ac.jp
2 Department of Bridge and Road Engineering, National University of Civil Engineering, 55 Giai Phong, Hai Ba Trung District, Hanoi 11616, Vietnam
* Correspondence: s167005@stn.nagaokaut.ac.jp

Received: 31 December 2019; Accepted: 4 February 2020; Published: 6 February 2020

check for updates

Abstract: The shield tunneling method is widely used, especially in urban areas, since it is efficient for minimizing disturbances to surroundings. Although segmental lining is commonly used in this method, in both the research and practice of tunnel lining design, the interaction between the ground and lining in the tangential direction remains unclear; that is, the mobilizing shear stress due to load models and the degree of the bond in the tangential direction. Therefore, to clarify the effects and mechanism of the tangential ground–lining interaction on segmental lining behavior, a parameter study was carried out, taking tangential spring stiffness, load models, soil stiffness, and shallow and deep tunnels as parameters. The interaction conditions were based on the existing literature. It was found that (1) the tangential spring has small effects on lining behavior, (2) the load model significantly affects the sectional forces, (3) the initial tangential earth pressure and slip ground–lining boundary provide more safety from a design viewpoint, and (4) in the case of shallow tunnels in soft ground, tensile stress appears in the lining. Therefore, it is important to take the tangential ground–lining interaction conditions into consideration during tunnel lining analysis.

Keywords: shield tunnelling; segmental lining design; ground–lining interaction; beam-spring model; parameter study

---

1. Introduction

The shield tunneling method is widely used in soft soils especially in urban areas because it is efficient for minimizing disturbances to surroundings. In this method, segmental lining is commonly used. The segmental lining is a connection of segments by longitudinal joints and circumferential joints, and its stability is ensured by the surrounding ground. There is interaction between the lining and the surrounding ground, constraining the lining in both normal and tangential directions. This mechanism results in reactions from the ground in both directions.

A segmental lining design is carried out for (1) transient situations before segment installation, during tunnel boring-machine (TBM) tunneling, and during additional temporary works; (2) persistent situations due to the ground and groundwater, tolerance of construction, surrounding load conditions, and tunnel-use conditions; (3) accidental situations; and (4) seismic situations [1]. This study focuses on the final loading stage due to the ground and groundwater since it is a critical stage especially in soft soils and shallow depth conditions. In the case of the segmental lining design for the final loading stage, the following two methods are commonly used.

The first approach involves analytical solutions [2–8], where the lining is modeled by a continuous beam without longitudinal joints and circumferential joints, and the ground is modeled by springs or a continuum medium. In these analytical solutions, initial earth pressure is applied directly on the lining, and then the ground reaction to the lining due to its deformation is assessed. This approach is fast and simple to use. However, it cannot take the complexity of a tunnel into account such as the aforementioned joints and effects of tunnel construction. In addition, linear elastic behaviors of lining and ground are assumed for the analytical solution.

The second approach is to use numerical analysis. The segmental lining is usually modeled by the beam-spring model, as shown in Figure 1a, which can consider the effect of a staggered arrangement of segments under the following assumptions: (1) the plane strain conditions in the transverse section for the lining and ground, (2) the linear-elastic behavior of the lining, and (3) the non-tension linear-elastic characteristic of the ground.

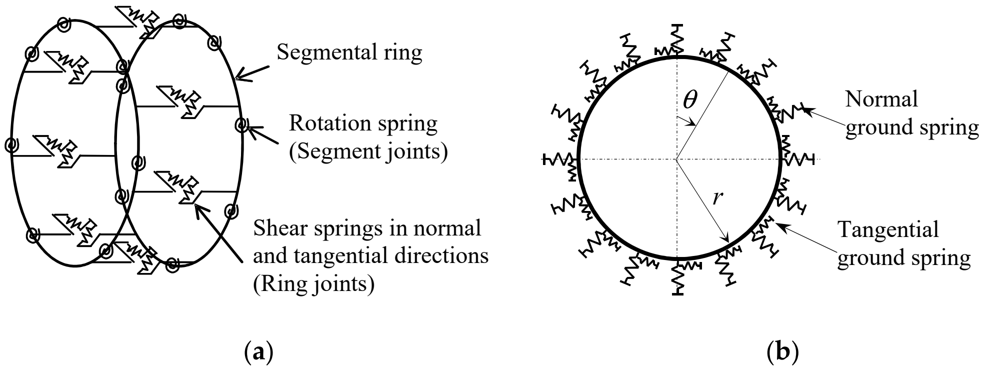

Figure 1. Analysis model. **(a)** Beam-spring model; **(b)** Ground spring model.

The two rings are connected by circumferential joints, which are modeled by shear springs in the normal and tangential directions. The segments are connected by a longitudinal joint, which is modeled by a rotational spring representing the relationship between the rotational angle and moments, and is tied at both ends of the segments. The ground is modeled by continuum elements or ground springs in the numerical analysis. The first ground model uses soil continuum elements and ground–lining interface elements to represent the surrounding ground and the ground–lining interaction, respectively [9–14]. This model can analyze both lining and ground behavior, and offer the ability to model sophisticated properties of ground and lining structure, construction process, and complex scenarios; that is, material non-linearity, different geological strata, gap-filling process, and effects on adjacent structures. However, it is difficult to simulate their behavior in shallow tunnels in soft ground, needs a lot of computational effort, and is time-consuming. The second ground model represents the ground–lining interaction by the ground spring, as shown in Figure 1b. The initial earth pressures in the normal and tangential directions are loaded directly onto the lining. This model can only analyze lining behavior, but is commonly applied in tunnel lining design as recommended by most current tunnel lining design standards [1,15–22] and in research such as [23–28].

In the case of the ground spring model, the initial earth pressure acting on the lining can be modeled by two common load models, as shown in Figure 2. Load model type 1 in Figure 2 is composed of horizontal and vertical earth pressure [15,17,21,23–25,29], which generate shear stress at the boundary between the ground and lining, while load model type 0 in Figure 2 only considers normal earth pressure [7,15]. The normal ground spring defines ground reactions in the normal direction against the lining and usually represents only the passive side of earth pressure [15,22–25,30]. The ground reaction curve (GRC), which can represent the ground reaction from the active side to the passive side and can include the Winkler spring model, was developed in consideration of the initial displacement of the excavation surface [31]. On the other hand, while the boundary between the ground and lining for a conventional tunnel is always regarded as full bond, for a shield tunnel the tangential ground spring stiffness, k_t, is commonly chosen in a range between 0 and the normal ground spring stiffness, k_n, as shown in Table 1. In the case of $k_t \cong 0$, which means the tangential slip between the ground and lining, the tangential spring is chosen to stabilize the computation [19,22]. In tunnel design practice, combinations of the load model types in Figure 2 and values of k_t in Table 1 are in use. Furthermore, it is noted that load model type 1 contradicts the ground–lining interaction model with small k_t, since the generated tangential stress in the case of load model type 1 is not fully transmitted onto the lining surface.

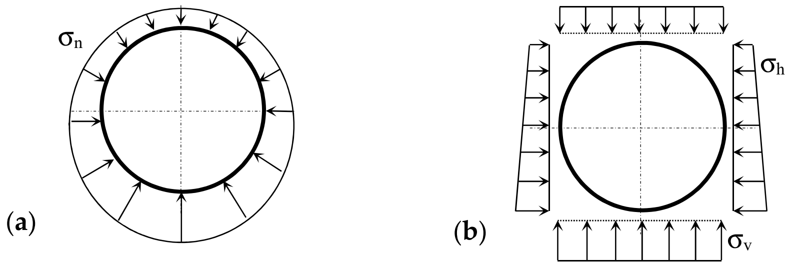

Figure 2. Load models for the lining analysis. **(a)** Type 0: Normal earth pressure; **(b)** Type 1: Vertical and horizontal earth pressure.

Table 1. Stiffness of the tangential spring between the ground and lining.

Value	References
$k_t \cong 0$	[7,15,19,20,22,23,28,29]
$k_t = k_n/3$	[15,21,23,26,32,33]
$k_t = k_n$	[11,14,34]

Note: k_t is the tangential spring constant per unit area.

Since the ground–lining interaction is one of the most crucial factors influencing the results of the analysis, the effect of the ground–lining interaction in the normal direction has been investigated intensively, but studies on the role of the ground–lining interaction in the tangential direction are few. Duddeck H. and Erdman J. [6] carried out parameter studies on the effect of tangential boundary condition between the ground and lining using analytical solutions without longitudinal and circumferential joints. Kimura S. et al. [27] carried out a parameter study on the effect of tangential spring stiffness, normal spring stiffness, the lateral earth pressure ratio and the overburden load using the beam-spring model with ground springs, to simulate the site measured data; that is, a specific case. Moreover, according to the literature review mentioned above, there exists a great disparity in using load models and boundary conditions in both research and practice of tunnel lining design. Therefore, this paper aims to make clear the effects of the tangential ground–lining interaction, of which the conditions come from the standards, guidelines, and recommendations on tunnel lining design, on the lining behavior and lining sectional forces, obtained through a parameter study using the beam-spring model and ground springs. This parameter study includes the initial tangential earth pressure, tangential ground spring stiffness, normal ground spring stiffness (covering a wide range between soft ground and stiff ground), and overburden load (representing deep and shallow tunnels). The results obtained contribute to our understanding on effects of tangential ground–lining interaction; thus, giving guidelines and information for practitioners regarding the tunnel lining design.

2. Methodology

The analysis method used in this research is composed of a beam-spring model as a lining model and a ground spring model with non-linear characteristics as a ground–lining model. The model has been validated by the site data and parameter study [28].

2.1. Lining Model

In the beam-spring model, the spring constants of the circumferential joints in the normal direction, k_{sr}, and the tangential direction, k_{st}, were determined by [15]:

$$k_{sr} = \frac{192EI_t}{(2b)^3} \tag{1}$$

$$k_{st} = \frac{2L_j hG}{b} \tag{2}$$

where E and G are the Young and shear moduli of the segment concrete, respectively; I_t is the moment of inertia for the area for one joint; L_j is the length between the consecutive joints; and b and h are the segment width and height, respectively.

The spring constant of the longitudinal joints, k_θ, was determined by [35]:

$$k_\theta = k_\theta^* \frac{EI_Z}{r} \tag{3}$$

where k_θ^* is a coefficient based on joint type (1 is used here), I_z is the moment of inertia, and r is the tunnel radius.

2.2. Ground–Lining Interaction

The ground spring for the ground–lining interaction is composed of the normal spring and the tangential one. The deformation characteristics of normal ground springs were determined based on the GRC, as shown in Figure 3. The shape of the GRC, which represents the non-linear characteristics of the ground, has been validated by the two-dimensional elasto-plastic finite element (FE) analysis [31]. Furthermore, the GRC has been applied to some similar targets successfully [36]. The GRC represents the normal ground–lining interaction from the active to the passive side, including ground self-stabilization.

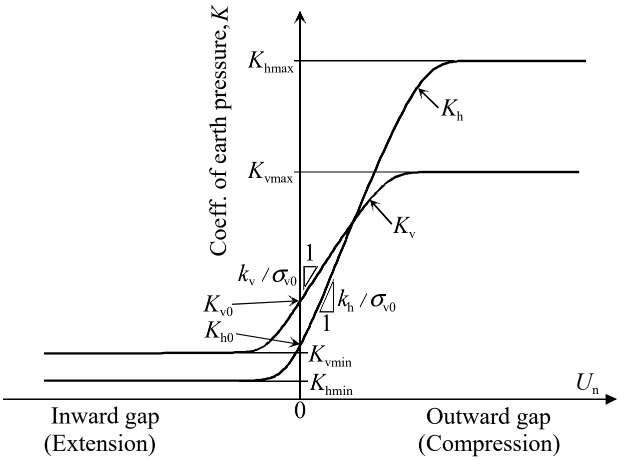

Figure 3. Ground reaction curves (GRC).

The GRC in the horizontal and vertical directions is formulated as follows:

$$K_i(u_n) = \begin{cases} (K_{i0} - K_{i\ min})\tanh\left(\frac{a_i u_n}{K_{i0} - K_{i\ min}}\right) + K_{i0} & (u_n \le 0) \\ (K_{i0} - K_{i\ max})\tanh\left(\frac{a_i u_n}{K_{i0} - K_{i\ max}}\right) + K_{i0} & (u_n \ge 0)\ (i = h, v) \end{cases} \tag{4}$$

where K is the coefficient of earth pressure; subscripts h and v show the horizontal and vertical directions, respectively; and subscripts 0, max, and min indicate K at rest and the upper and lower limits of K, respectively. Here, u_n is the gap from the original excavated surface before excavation to the outer surface of the lining. It is noted that ground self-stabilization and the constant overcut can be represented using the gap instead of the displacement, as shown in Figure 4. a is the normalized subgrade reaction coefficient k by the initial overburden load at spring line σ_{v0} at $u_n = 0$. The coefficient of earth pressure in the normal direction, K_n, can be interpolated between K_h and K_v by the angle measured from the crown to the considered point (Figure 1b). Then, the normal earth pressure acting on the lining, σ_n, can be obtained. The tangential ground spring, which transmits the load between ground and lining tangentially, was assumed to be linearly elastic.

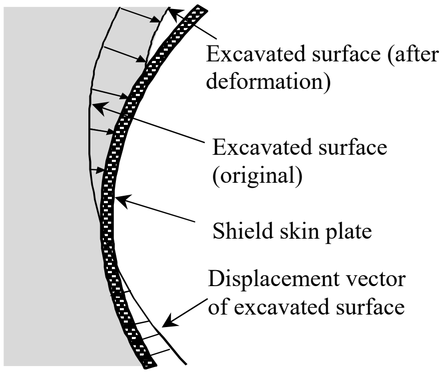

Figure 4. Displacement of the excavated surface.

2.3. Initial Stress State

In the case of soft ground, arching action of the ground is not expected, while in the case of stiff ground, the normal earth pressure acting on the lining becomes close to 0 when the ground moves to the active side. The aforementioned GRC can represent both phenomena. Therefore, loosening earth pressure for the vertical pressure is not adopted in this study.

The initial earth pressure along the lining in the normal and tangential directions, σ_{n0} and τ_0, are calculated from the vertical and horizontal earth pressure at rest, σ_{v0} and σ_{h0}, as follows:

$$\sigma_{n0} = \sigma_{v0} \cos^2 \theta + \sigma_{h0} \sin^2 \theta \quad (5)$$

$$\tau_0 = (\sigma_{v0} - \sigma_{h0}) \sin \theta \cos \theta \quad (6)$$

where θ is shown in Figure 1b. Load model type 0/type 1 in Figure 2 correspond to the load model on the lining without/with the initial tangential earth pressure, τ_0, respectively. Here, it is noted that the effective earth pressure method can be used instead of the total earth pressure method as follows: the water pressure is applied to the lining directly, and the effective earth pressure is in use.

2.4. Parameter Study

Table 2 presents all analysis cases. The tangential spring constant, k_t, was defined by three different methods according to Table 1 and was used as a parameter. The initial tangential earth pressure, τ_0, was taken as a parameter; that is, with and without the initial tangential earth pressure, τ_0, as shown in Figure 2. Various ground stiffness, from soft ground to stiff ground, were considered since this has a considerable influence on lining behavior. Here, the coefficients of the subgrade reaction in both the vertical and horizontal directions were assumed to be equal: $k_v = k_h = k_n$. The overburden depth, h, was selected to represent a shallow tunnel and a deep tunnel because the lining behavior changes under different overburden depths.

Table 2. Analysis cases of the parameter study.

Case	k_t/k_n	Load Model	Coefficient of Subgrade Reaction, MN/m^3	Overburden Depth, m
10	0	Type 0 (no τ_0)	10, 50, 100, 500, 1000	7.870, 37.635
20	1/3			
30	1			
11	0	Type 1 (with τ_0)		
21	1/3			
31	1			

3. Analysis Conditions

3.1. Site Data

Geotechnical data from the Neyagawa tunnel site in Japan [28] were used for this analysis. The dimensions and material properties of the lining are presented in Table 3. The joint spring constants were calculated by Equations (1) to (3). The segmental ring was assembled from eight precast concrete segments connected by longitudinal joints, and the consecutive rings were in a staggered arrangement, as shown in Figure 5. The tunnel position and soil properties are shown in Table 4. The Neyagawa tunnel is a deep tunnel where the overburden depth, h, is 37.635 m; the tunnel diameter, D, is 7.87 m; and the overburden ratio, h/D, is 4.78 with a groundwater level of GL-7.126 m. In this study, a shallow tunnel with an overburden depth of 7.87 m (h/D = 1.00), was also considered. $K_{hmin} = K_{vmin} = 0.0$ was assumed so that ground self-stabilization was expected as demonstrated in Figure 3. The K_{hmax} and K_{vmax} values were assumed to be 5.0 based on previous research [31].

Table 3. Segmental lining dimensions and material properties.

Radius (m)	3.935
Thickness (m)	0.370
Width (m)	1.000
Density (kN/m^3)	28.000
Elastic modulus (GN/m^2)	33
Poisson ratio	0.2
Segment joint spring, k_θ (MNm/rad)	35.4
Ring joint spring in normal dir., k_{sr} (MN/m)	827
Ring joint spring in shear dir., k_{st} (MN/m)	1260

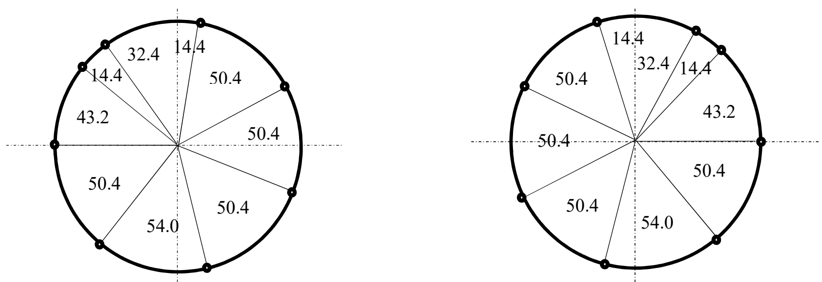

(**a**) Even-number rings (**b**) Odd-number rings

Figure 5. Staggered arrangement of segments.

Table 4. Tunnel position and ground properties.

Ground Properties	Deep Tunnel	Shallow Tunnel
Overburden depth (m)	37.635	7.870
Groundwater level (m)	GL-7.126	GL-7.126
Submerged density (kN/m^3)	5.500	5.500
Vertical effective earth pressure at crown (kN/m^2)	342.27	127.84
Water pressure at crown (kN/m^2)	300.80	9.10
Coef. of earth pressure $K_{h\ min}$, K_{h0}, $K_{h\ max}$	0.0, 0.5, 5.0	0.0, 0.5, 5.0
Coef. of earth pressure $K_{v\ min}$, K_{v0}, $K_{v\ max}$	0.0, 1.0, 5.0	0.0, 1.0, 5.0

Figure 6 shows the distributions of the initial normal and tangential earth pressure at rest and the water pressure around the tunnel ring. This figure shows that the shear components are not small, as they are about 0% to 35% of the normal effective ones for both tunnels.

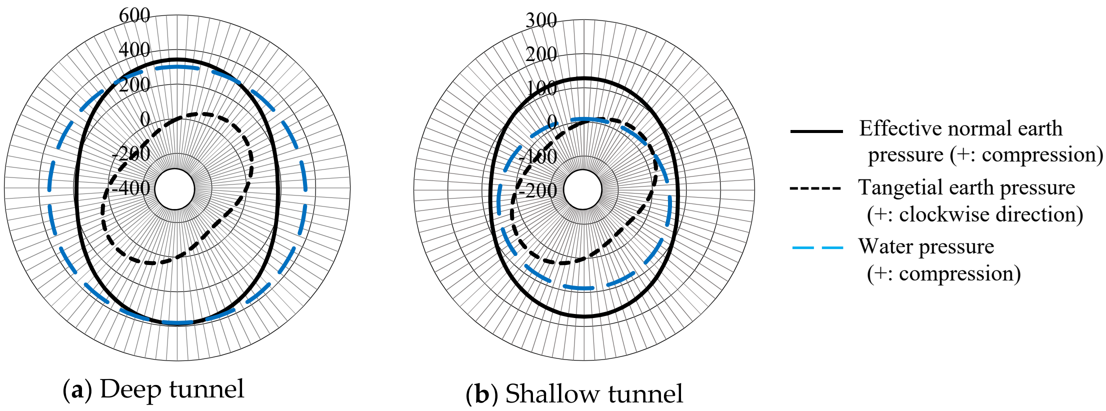

Figure 6. Distribution of initial earth pressure and water pressure on the lining (kN/m^2).

3.2. Analysis Model

The lining was divided into 100 beam elements with 100 nodes. To simulate the ground–lining interaction, two-node springs were used. These springs were connected to the lining at the inner end, and the outer end was fixed outside. In this study, the effective earth pressure method was used. To represent the GRC in Figure 3, the initial normal effective earth pressure at $u_n = 0$ was set in the ground spring as a prestress load, and the shape of the ground reaction curve is represented by multi–linear relationship between the gap and spring constant of the ground spring. It is noted that $K_{h\ min} = K_{v\ min} = 0$ in Figure 3 represents the non-tension characteristics of the ground; that is, ground self-stabilization. The initial tangential earth pressure was applied to the tangential ground springs as a prestress load, and the water pressure was placed directly on the lining in the normal direction. For the analysis, the finite element solver DIANA [37] was used. The sign definitions in this study are as follows: the bending moment M (+: convex deformation to outside); the axial force N (+: compression force); the gap from the initial excavation surface to the lining in the normal direction u_n (+: toward the outside from the tunnel); and the tangential displacement of the lining u_t (+: displacement to counterclockwise).

4. Results and Discussion

The influence of each interaction condition on lining behavior was investigated. The results from the even-numbered ring are used because of the bisymmetric results at both rings, which are due to the bisymmetric allocation of longitudinal joints in the analysis model as shown in Figure 5. The lining displacement, the normal effective earth pressure, the tangential earth pressure acting on the lining, the bending moment, and the axial force are shown in Figures 7 and 8 for the deep tunnel and shallow tunnel for the ground at k_n = 10, 100, 1000 MN/m^3 only because the trends of the results for the ground at k_n = 50, 500 MN/m^3 are similar to the others.

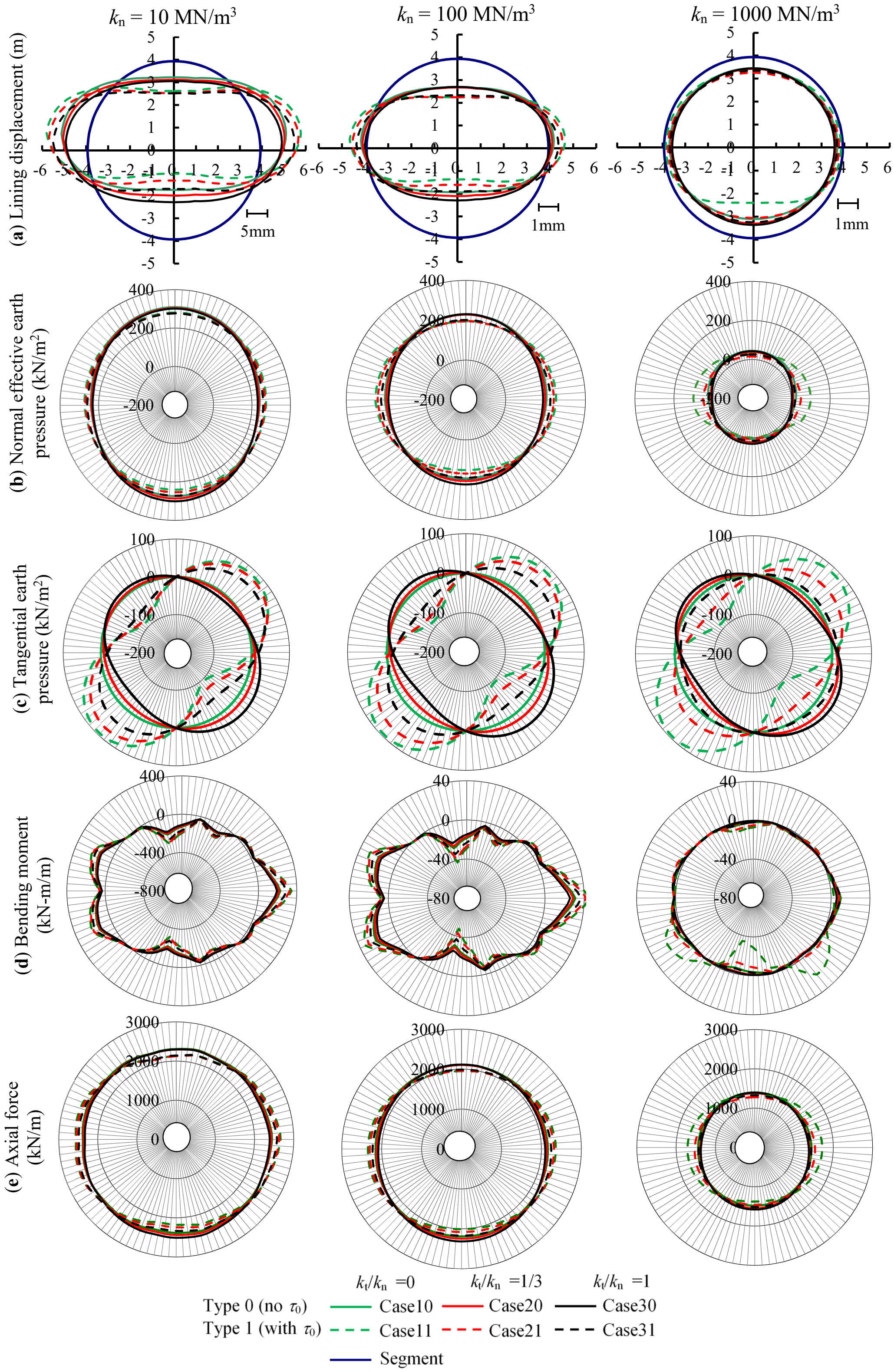

Figure 7. Lining displacement and ground reactions (deep tunnel).

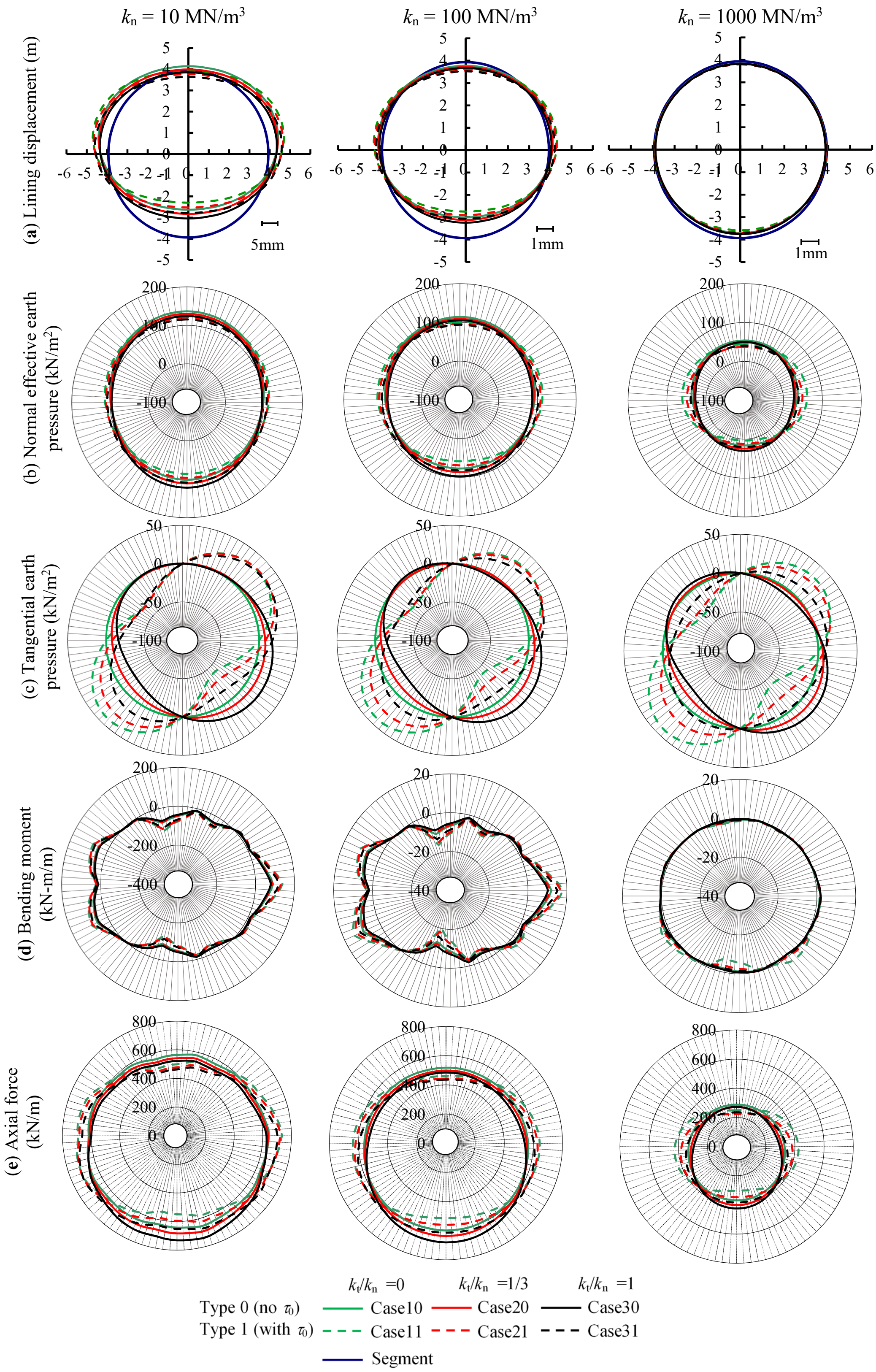

Figure 8. Lining displacement and ground reactions (shallow tunnel).

4.1. Lining Behavior and Earth Pressure Acting on Lining

4.1.1. Lining Displacement

From the lining displacement in Figures 7a and 8a, the following was found:

1. Generally, the lining deformation shape is flat in the horizontal direction and moves upward. This is due to the followings: (1) the initial effective earth pressure in the vertical direction is larger than that in the horizontal direction because K_{h0} = 0.5 in this analysis, and (2) the buoyancy is larger than the lining self-weight.
2. As the tangential spring constant, k_t, increases, the lining shape becomes more circular; that is, the lining deformation becomes smaller. This is because the tangential springs reduce the lining displacement in the tangential direction, and their restraint increases as k_t increases.
3. Compared with load model type 0 (initial shear stress τ_0 = 0) the lining at load model type 1 deforms more in the horizontal direction. This is because τ_0 compresses the lining in the vertical direction and extends it to the horizontal direction at K_{h0} = 0.5.
4. As the coefficient of the subgrade reaction, k_n, increases, the lining shape becomes more circular. This is because the ground reaction force restricts the lining deformation in the horizontal outward direction and increases with larger k_n.
5. Compared with the shallow tunnel, the lining in the deep tunnel deforms more in the horizontal direction, and the diameter of the lining decreases. This is because as the overburden depth increases, (1) the larger difference between the initial vertical effective earth pressure and the initial horizontal effective earth pressure requires more lining deformation to redistribute the effective earth pressure, and (2) the increase in water pressure causes more shrinkage of the lining.

4.1.2. Normal Effective Earth Pressure

The normal effective earth pressure, σ'_n can be obtained from the gap from the original excavated surface before excavation to the outer surface of the lining, u_n. Therefore, the σ'_n tendency can be explained by u_n. Usually, u_n is equal to the displacement of the excavated surface in the normal direction except the existing gap between the excavated surface after excavation and the outer surface of the lining because of ground self-stabilization as shown in Figure 4. In this study, the self-stabilization of the ground occurs only at k_n = 1000 MN/m^3 and in the deep tunnel.

From the normal effective earth pressure along the lining, σ'_n in Figures 7b and 8b, the following was found:

1. The distribution shape of σ'_n is more circular than that of the initial normal effective earth pressure, σ'_{n0}. This comes from the redistribution of σ'_n due to the lining stiffness. Furthermore, σ'_n is close to 0 around the invert at k_n = 1000 MN/m^3 and in the deep tunnel. This is because (1) the high water pressure causes the shrinkage of the segmental ring, (2) the large k_n reduces the normal displacement of the excavated surface due to ground self-stabilization, and (3) the buoyancy, which is larger than the self-weight of the lining, lifts the lining.
2. As k_t decreases and the load model changes from type 0 to type 1, the distribution shape of σ'_n becomes more flat in the horizontal direction. These trends reflect the lining displacement.
3. As k_n increases, σ'_n decreases and the distribution shape of σ'_n becomes more flat in the horizontal direction. This is because (1) the high water pressure in the deep tunnel reduces the lining diameter, (2) a larger k_n decreases σ'_n under the same displacement in the active side, and (3) as k_n increases, the σ'_n around the invert and crown decreases more than the σ'_n at the spring line under the displacement in the active side because K_{h0} = 0.5.
4. For $k_n \leq$ 100 MN/m^3, the σ'_n at the deep tunnel is larger than that at the shallow tunnel, and for k_n = 1000 MN/m^3, the tendency of σ'_n is the reverse. This is because (1) the deeper tunnel has the larger initial normal effective earth pressure, σ'_{n0} and the larger water pressure, σ_w, and (2) a higher σ_w reduces the lining diameter and σ'_n more, especially for k_n = 1000 MN/m^3.

4.1.3. Tangential Earth Pressure

From the tangential earth pressure, τ, around the lining in Figures 7c and 8c, the following was found:

1. The shape of the τ distribution is an ellipse whose major axis has an angle of 45 degrees against the vertical axis, as the loads acting on the lining and the lining structure are almost biaxially symmetric against the horizontal and vertical direction.
2. As k_t increases, (1) for load model type 1 (with τ_0), the distribution shape of τ becomes more circular than that of the initial tangential earth pressure, τ_0, which corresponds to τ under k_t/k_n = 0; and (2) for load model type 0 (no τ_0), the distribution shape of τ becomes more flat than that of τ = 0, which corresponds to τ at k_t/k_n = 0; and (3) the load model type, that is, the initial tangential earth pressure, τ_0, has more effect on the tangential earth pressure, τ. This is due to the following: (1) the shear stress magnitude is proportional to relative displacement and k_t. Shear stress is generated in the opposite direction of the relative displacement of the lining against the ground. Under the analysis conditions of this study, the relative displacement direction is horizontally outward, as shown in Figures 7a and 8a. (2) The direction of the initial tangential earth pressure, τ_0, for load type 1 in Figure 2 under $K_0 < 1$ is also in the horizontal outward direction. (3) The calculated τ comes from the superposition of the above shear stresses.
3. As k_n increases, (1) for k_t/k_n = 0, the shape of the τ distribution is almost the same, and (2) for k_t/k_n > 0, it becomes more circular. This is because, as k_n increases, (1) the lining deformation decreases because of the increase in ground reaction force; (2) k_t increases for $k_t/k_n > 0$; and finally, (3) the relative displacement between the lining and ground decreases, as shown in Figures 7a and 8a.
4. The τ of the deep tunnel is larger than that of the shallow tunnel. This is because the overburden load increases, (1) the relative displacement between lining and ground is larger, as shown in Figures 7a and 8a; and (2) for load model type 1, the initial tangential earth pressure, τ_0, is larger.

4.2. Cross-Sectional Forces

4.2.1. Bending Moment

Figures 7d and 8d show the distribution of bending moment M for the deep tunnel and the shallow tunnel. To make each parameter's effect clear, Figure 9 shows the maximum and minimum moment (M_{max}, M_{min}), respectively. From these figures, the following was found:

1. The distribution shape of M is flat in the horizontal direction.
2. The distribution shape of M becomes more uniform as k_t and k_n increase, load model type 0 is compared with load model type 1, and the overburden decreases.
3. For $k_n \leq 100$ MN/m^3, the maximum value of the absolute M shows a maximum of a 23% reduction as k_t/k_n increases from 0 to 1, and they show approximately a 58% increment as the load model changes from type 0 to type 1. For $k_n \geq 500$ MN/m^3, the magnitude of M becomes close to zero. This can be explained as the same as in Section 4.1.1 (Lining Displacement) since the distribution of M basically reflects the lining deformation in Figures 7a and 8a.
4. The M at the longitudinal joints of the ring is close to 0; on the other hand, around these longitudinal joints, the M in the next ring has a maximum/minimum value, especially $k_n \leq 100$ MN/m^3. This is because (1) the bending stiffness of the longitudinal joints is smaller than that of the segment itself, and (2) a certain moment in one ring is transferred through the next ring by the circumferential joints in the case of a staggered arrangement.
5. In the case of the deep tunnel, a very stiff ground (k_n = 1000 MN/m^3), k_t/k_n = 0, and load model type 1, M fluctuates significantly at the lower part while in other cases, the M distributions are more stable. This is because (1) when k_t/k_n = 0 and the load model is type 1 (with τ_0), the lining deforms most flat in the horizontal direction; (2) when k_n is larger, ground self-stabilization is

expected with a small active displacement; (3) in the deep tunnel, high water pressure causes lining shrinkage; that is, the displacement in the active side appears; (4) because of buoyancy, the tunnel moves upward; (5) the segments are installed in staggered arrangements; and (6) therefore, while the upper part of the lining is supported by the ground, the lower part of the lining can move freely in the normal direction because of the gap between the lining and ground, as shown in Figure 10 which presents the lining displacements in the normal and tangential directions, u_n and u_t, in the case of k_n = 1000 MN/m^3 in the deep tunnel. Thus, M has peaks at the longitudinal joints of the next rings at the lower part.

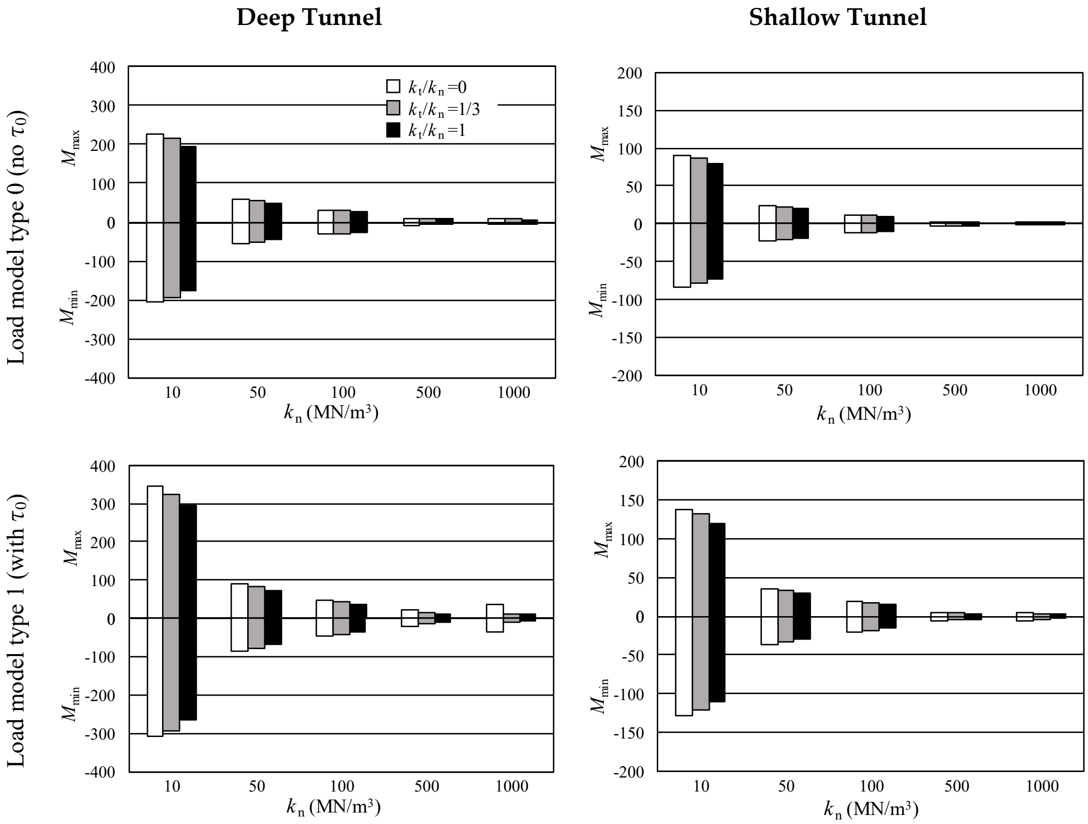

Figure 9. Maximum and minimum bending moment (kN-m/m).

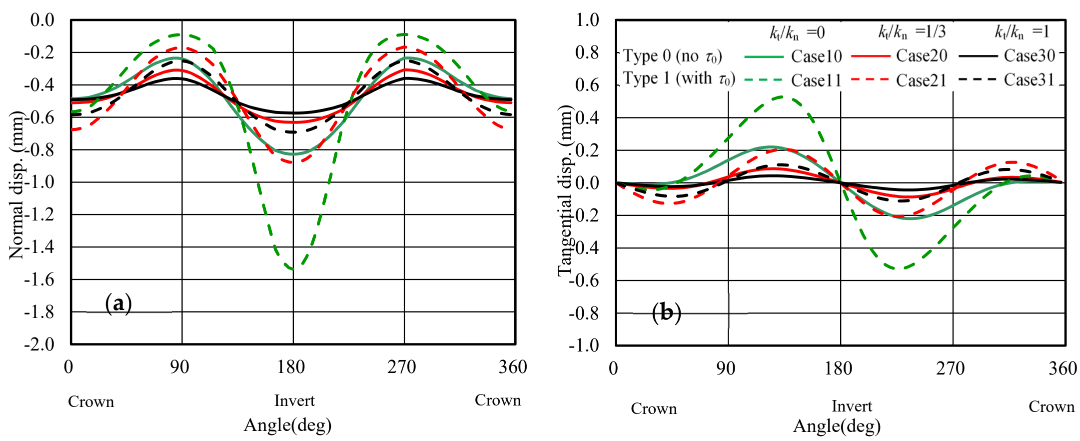

Figure 10. Lining displacement for ground at k_n = 1000 MN/m^3 (deep tunnel). (**a**) Normal displacement (+: outward); (**b**) Tangential displacement (+: counterclockwise).

4.2.2. Axial Force

The axial force in the segmental lining, N, results from the normal force on the lining, such as normal effective earth pressure and water pressure; the tangential force on the lining, such as the tangential force due to the tangential springs and the tangential earth pressure due to the load model; and the vertical force due to the self-weight of the lining. Therefore, the axial force distribution is determined by the normal effective earth pressure described in Section 4.1.2, the tangential earth pressure described in Section 4.1.3, the water pressure, and the self-weight of the lining.

Figures 7e and 8e show the distribution of axial force for the deep tunnel and the shallow tunnel, respectively. To make each parameter's effect clear, Figure 11 shows the maximum axial force $N_{\max}$, and Figure 12 shows the F_h/F_v ratio defined as follows:

$$\frac{F_h}{F_v} = \frac{N_C + N_I}{N_L + N_R} \tag{7}$$

where N_L, N_R, N_C, and N_I are axial forces in the lining at the left and right spring line, crown, and invert, respectively. F_h/F_v shows the shape of the axial force distribution, which becomes horizontally long for $F_h/F_v < 1$ and vertically long for $F_h/F_v > 1$. From these figures, the following was found:

1. The distribution shape of N is flat in the horizontal direction, while that of σ_n' is flat in the vertical direction. This is because the N comes from the σ_n' initial tangential stress τ_0, tangential stress τ due to k_t, water pressure σ_w, and the self-weight of the lining.
2. As the tangential spring stiffness, k_t, increases, F_h/F_v increases; that is, the distribution shape of N deforms to the vertical outward direction and the horizontal inward direction. This is because the tangential spring restricts the lining deformation to be flat in the horizontal direction under K_{h0} = 0.5, and it causes compression force to the lining in the horizontal direction and tensile force to the lining in the vertical direction.
3. As the load model changes from type 0 to type 1, F_h/F_v decreases; that is, the distribution shape of N changes from being flat in the vertical direction to being flat in the horizontal direction. This is because the shear earth pressure generates shear force on the lining to the horizontal outward direction, and this causes an increase in N in the vertical direction and a decrease in N in the horizontal direction. This tendency is the reverse of that caused by k_t.
4. The coefficient of subgrade reaction k_n and the overburden depth influence the magnitude of $N_{\max}$ in Figure 11 but do not affect the distribution shape of N as shown in Figures 7 and 8. This can be explained the same way as σ_n' in Section 4.1.2 (Normal Effective Earth Pressure).
5. As for $N_{\max}$ in Figure 11, as k_t increases, $N_{\max}$ increases for load model type 0, and $N_{\max}$ decreases for load model type 1. This is because $N_{\max}$ appears at the invert for load model type 0 and at the spring line for load model 1, as shown in Figures 7, 8 and 12, and the influences of k_t on F_h and F_v are reversed.
6. As k_n increases and overburden depth decreases, $N_{\max}$ in Figure 11 decreases. This can be explained the same way as σ_n' in Section 4.1.2 (Normal Effective Earth Pressure).
7. While the N distribution becomes smoother as k_n increases, the N distribution bends at the segment joints of the next rings in the case of k_n = 10 MN/m^3. This can be explained as follows: with lower k_n, (1) the deformation of the lining is larger, (2) the bending angle at the segment joint increases since the bending stiffness at the segment joints is smaller than that of the segment section, and (3) a larger compression strain is generated at the segment joints of the next ring; that is, a larger N appears.
8. In the case of k_n = 1000 MN/m^3, k_t/k_n = 0 and load model type 1, the N around the spring line is larger than the N at other positions (F_h/F_v is smallest). This is because (1) no constraint occurs in the tangential direction due to k_t/k_n = 0, (2) σ_n' is close to 0 as explained in Section 4.1.2 (Normal Effective Earth Pressure), and (3) the initial earth pressure τ_0 due to load model type 1 and the self-weight of the lining generate the N directly.

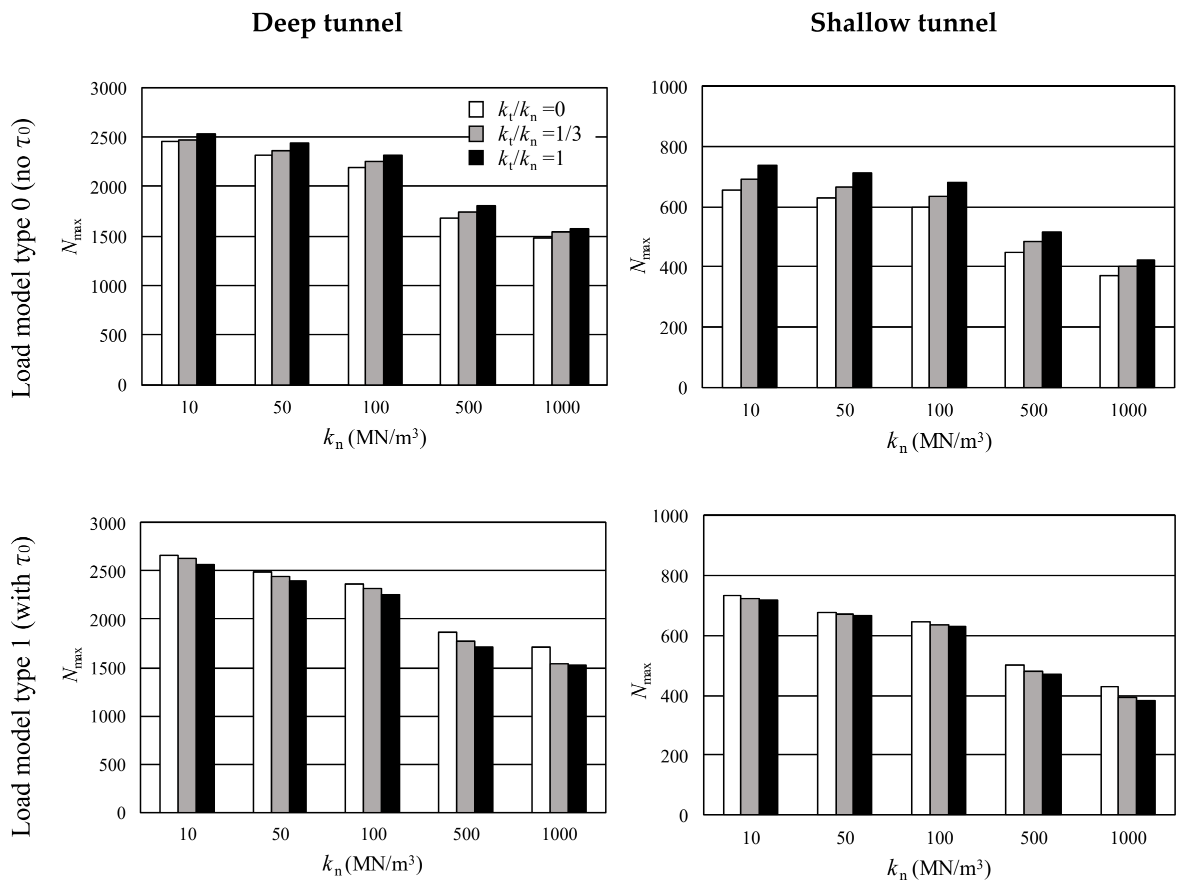

Figure 11. Maximum axial force (kN/m).

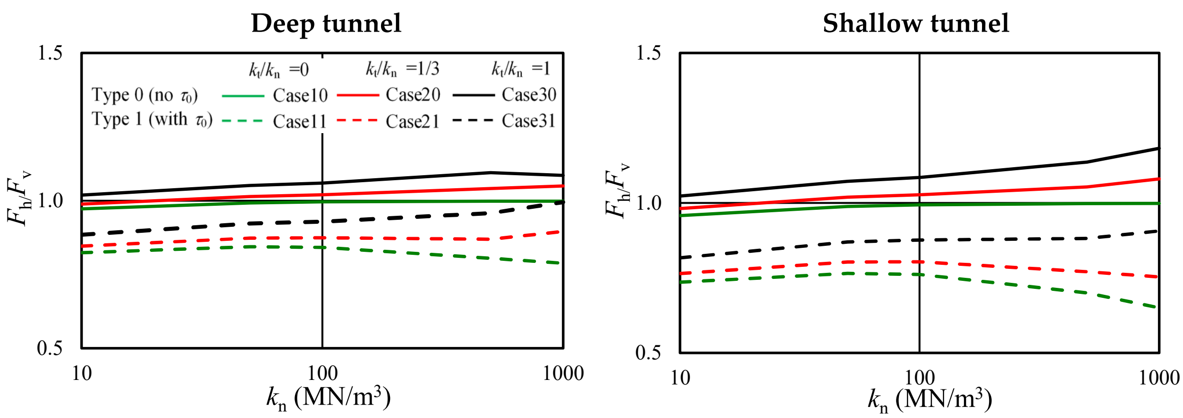

Figure 12. F_h/F_v.

4.2.3. Normalized Eccentricity

The eccentricity e normalized by the segment thickness t is used to evaluate the effects of the parameters on the sectional forces. The eccentricity e is defined as:

$$e = \frac{M_{max}}{N_{assoc}} \tag{8}$$

where M_{max} is the maximum moment and N_{assoc} is the associated axial force at M_{max}. When e/t is larger than 1/6 (≅ 0.167), tensile stress appears in the segment.

Figure 13 shows the e/t for the deep tunnel and the shallow tunnel, respectively. From Figure 13, the following was found:

1. e/t is larger than 0.167 at k_n = 10 MN/m^3 for the deep tunnel and at k_n < 50 MN/m^3 for the shallow tunnel, while e/t is negligibly small at $k_n \geq$ 500 MN/m^3. These are the results of the M distribution and N distribution in Figures 7 and 8. This indicates that earth pressure should be considered carefully in soft soils for a shallow tunnel, since tensile stress appears in the lining.
2. As the tangential spring constant, k_t/k_n, increases from 0 to 1, e/t decreases, but the change is less than 0.05. This indicates that the influence rate of k_t on M_{max} and N_{assoc} is similar, and the effect of k_t on e/t is limited.
3. As the load model changes from type 0 to type 1 under e/t > 0.167, e/t increases by about 1.4 times for the deep tunnel and about 1.7 times for the shallow tunnel. This indicates that the load model type (i.e., τ_0) influences e/t significantly.
4. With larger k_n, e/t is drastically reduced. This means that absolute M_{max} decreases more than N_{assoc} as k_n increases.
5. The e/t of the shallow tunnel is at most about 1.6 times the e/t of the deep tunnel. This means that absolute M_{max} decreases less than N_{assoc} as the overburden depth h decreases, since the difference of the initial effective earth pressures at the crown and invert is constant, but the initial vertical effective earth pressure decreases as h decreases.

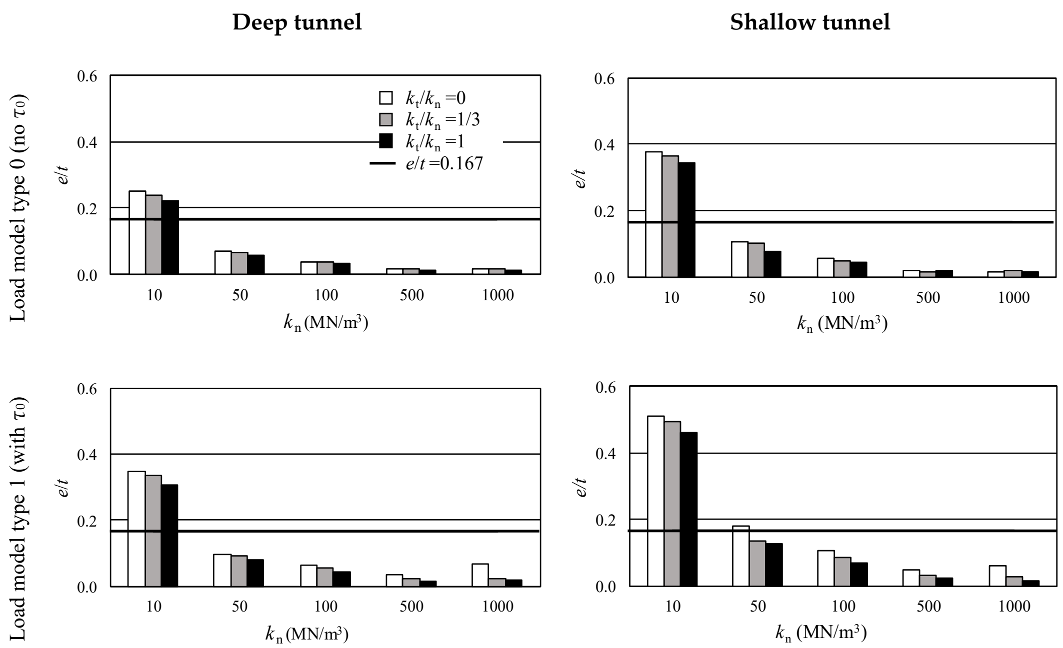

Figure 13. Normalized eccentricity.

4.2.4. Support Rate of the Initial Earth Pressure by the Lining

To make the influence of each parameter on the arching effect clear, Figure 14 shows the support rate of the initial effective earth pressure by the lining in the vertical and horizontal directions, r_v and r_h, defined as:

$$F_{i0} = \sigma'_{i0} \times D \ (\mathrm{i} = \mathrm{h},\ \mathrm{v}) \quad (9)$$

$$\begin{cases} F_{ev} = N_L + N_R - \sigma_w \times D - W/2 \\ F_{eh} = N_C + N_I - \sigma_w \times D \end{cases} \quad (10)$$

$$r_i = \frac{F_{ei}}{F_{i0}} \ (\mathrm{i} = \mathrm{h},\ \mathrm{v}) \quad (11)$$

where F_0 is the initial force on the tunnel section due to the initial effective earth pressure σ'_0; F_e is the force due to the effective earth pressure supported by the lining; N_L, N_R, N_C, and N_I are axial forces in the lining at the left and right spring lines, crown, and invert, respectively; σ_w is the water pressure at the tunnel center; D is the tunnel diameter; W is the self-weight of the lining; and the suffixes v and h show the vertical and horizontal directions, respectively. Here, in the case where the support rate of the initial effective earth pressure σ'_{i0} by the lining r_i (i = h and v) is less than 1, the rest of σ'_{i0} is expected to be supported by the surrounding ground. On the other hand, in the case where r_i (i = h and v) is larger than 1, the ground reaction force acting on the lining is larger than σ'_{i0}. For the deep tunnel, F_{v0} = 2864 kN/m and F_{h0} = 1432 kN/m, and for the shallow tunnel, F_{v0} = 1176 kN/m and F_{h0} = 588 kN/m.

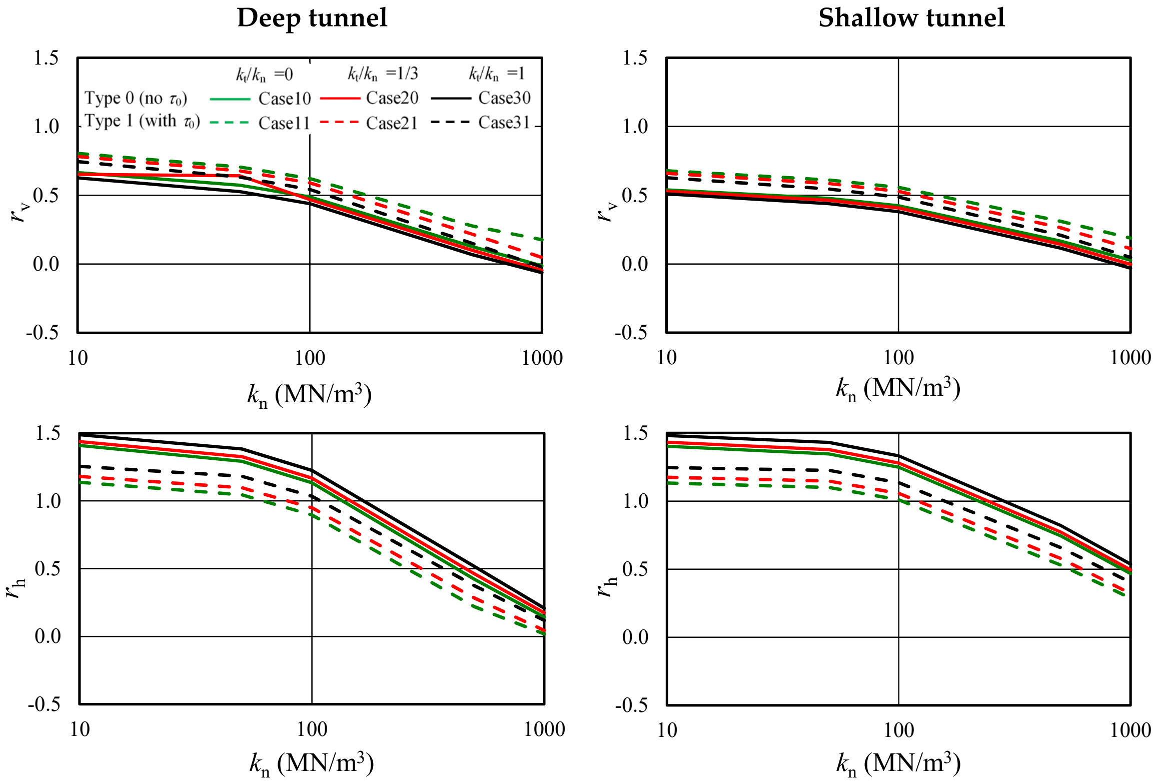

Figure 14. Support rate of initial effective earth pressure by lining in the vertical and horizontal direction r_v, r_h.

From Figure 14, the following was found:

1. $r_v < 1 < r_h$ is for $k_n \leq 100$ MN/m^3 while r_v is close to 0, and $r_h < 1$ for $k_n = 1000$ MN/m^3. This is because (1) for $k_n \leq 100$ MN/m^3, the effective earth pressure acting on the lining, σ'_n at the crown and invert are at the active side, and the σ'_n at the spring line is at the passive side due to the ground reaction, and (2) for $k_n = 1000$ MN/m^3, σ'_n is always at the active side and σ'_n is close to zero for the deep tunnel due to ground self-stabilization, as shown in Figures 7b and 8b.
2. As the tangential spring constant, k_t, decreases and the load model type changes from type 0 to type 1, r_v increases and r_h decreases. This tendency can be explained the same as in Section 4.1.3 (Tangential Earth Pressure).
3. As the coefficient of the subgrade reaction, k_n, increases, r_v and r_h decrease. This is because as k_n increases, σ'_n drops more in the active side as described in Section 4.1.2 (Normal Effective Earth Pressure). Furthermore, r_v and r_h have almost the same value for the deep tunnel and shallow tunnel. This means that the influence rate of the overburden depth on the initial effective earth pressure σ'_0 and the effective earth pressure σ'_n is almost the same in this analysis condition.

5. Conclusions

A parameter study was conducted to investigate the effects of the ground–lining interaction in the tangential direction on lining response, using the beam-spring model and ground springs. Tangential ground spring stiffness k_t, load model type (the initial tangential earth pressure, τ_0), normal ground spring stiffness k_n, and overburden depth h were used as parameters. As a result, the following was found:

1. The distribution of normal effective earth pressure acting on lining σ'_n mainly obtains the influence of k_n and h, and the distribution of tangential earth pressure acting on lining τ is influenced by k_t and the load model type (i.e., τ_0). Lining displacement is defined by σ'_n, τ, and buoyancy and determines the distributions of the bending moment, M. The distribution of N is determined by σ'_n, τ, water pressure σ_w, and the lining self-weight. The influence of each parameter is propagated through the above mechanism.
2. The k_t restricts the lining displacement in the tangential direction, and the axial force in the lining is generated in the opposite direction of the lining displacement. Therefore, as k_t/k_n changes from 0 to 1: (1) The lining shape and distribution shapes of M and N become more circular. (2) For $k_n \leq$ 100MN/m^3, the absolute M decreases at most to 23%. For $k_n \geq 500$ MN/m^3, the magnitude of M becomes close to zero. (3) The N_{max} changes within 5%. (4) The change of the normalized eccentricity, e/t, is less than 0.05.
3. The shear stress appears at the boundary toward the spring line for load model type 1 under $K_{h0} < 1$. Therefore, as the load model changes from type 0 to type 1, (1) the lining shape and distribution shapes of M and N become flat in the horizontal direction; (2) for $k_n \leq 100$ MN/m^3, the absolute M increases to at most 58%; (3) the N_{max} increases at most to 9%; and (4) under $e/t >$ 0.167, e/t increases 1.4 times for the deep tunnel and 1.7 times for the shallow tunnel. The case of $e/t > 0.167$, which means tensile stress appears in the lining, corresponds to $k_n = 10$ MN/m^3 for the deep tunnel and $k_n < 50$ MN/m^3 for the shallow tunnel. This indicates that the load model has significant effects on sectional forces, especially in shallow tunnels in soft soils.
4. As k_n increases, under the same displacement, the normal effective earth pressure σ'_n increases at the passive side and decreases at the active side. As a result, the lining shape and distribution shapes of M and N become more circular, and M, N, and e/t are drastically reduced at mboxemphk$_n \geq 500$ MN/m^3.
5. As the overburden depth, h, decreases, the effective earth pressure σ'_n and water pressure σ_w decrease, but the difference of the initial effective earth pressures at the crown and invert is constant. Then, (1) the lining shape and the distribution shape of M become more circular, (2) N decreases, and (3) e/t increases by about 1.6 times.
6. In the case of a shallow tunnel in soft soil where $e/t > 0.167$, tensile stress appears in the lining. Therefore, the tangential ground–lining interaction conditions, such as the initial tangential earth pressure due to load model and the tangential spring constant, should be considered carefully since these conditions significantly influence the bending moment in the segmental lining.
7. In the case where the support rates of the initial effective earth pressure by the lining in the vertical and horizontal direction, r_v and r_h, are less than 1, which means the existence of an arching effect (the support of partial initial effective earth pressure by the surrounding ground), this should be confirmed, especially in the case of a shallow tunnel in soft ground.

For further studies, it is recommended that the gap between the lining and the original excavation surface before excavation should be considered, since this factor will influence the normal earth pressure acting on the lining. Furthermore, the ground–lining interaction should be examined using in situ data.

Author Contributions: Conceptualization, A.T.P.; methodology, A.T.P and M.S.; software, A.T.P. and M.S.; validation, A.T.P. and M.S.; formal analysis, A.T.P.; writing—original draft preparation, A.T.P.; writing—review and editing, A.T.P and M.S.; supervision, M.S. All authors have read and agreed to the published version of the manuscript.

Funding: This research received no external funding.

Conflicts of Interest: The authors declare no conflict of interest.

References

1. BSI (British Standards Institute). *PAS 8810:2016: Tunnel Design—Design of Concrete Segmental Tunnel Linings—Code of Practice*; BSI: London, UK, 2016.
2. Morgan, H. A contribution to the analysis of stress in a circular tunnel. *Geotechnique* **1961**, *11*, 37–46. [CrossRef]
3. Schulze, H.; Duddeck, H. Spannungen in schildvorgetriebenen tunneln. *Beton-und Stahlbetonbau* **1964**, *59*, 169–175.
4. Muir Wood, A.M. The circular tunnel in elastic ground. *Geotechnique* **1975**, *25*, 115–127. [CrossRef]
5. Einstein, H.H.; Schwartz, C.W. Simplified Analysis for Tunnel Supports. *J. Geotech. Eng. Div.* **1979**, *105*, 499–517.
6. Duddeck, H.; Erdman, J. On structural design models for tunnels in soft soil. *Undergr. Space* **1985**, *9*, 246–259.
7. Matsumoto, Y.; Nishioka, T. *Theoretical Tunnel Mechanics*; University of Tokyo Press: Tokyo, Japan, 1991; p. 178.
8. Zhang, Z.; Zhang, M.; Jiang, Y.; Bai, Q.; Zhao, Q. Analytical prediction for ground movements and liner internal forces induced by shallow tunnels considering non-uniform convergence pattern and ground-liner interaction mechanism. *Soils Found.* **2017**, *57*, 211–226. [CrossRef]
9. El-Nahhas, F.; El-Kadi, F.; Ahmed, A. Interaction of tunnel linings and soft ground. *Tunn. Undergr. Space Technol.* **1992**, *7*, 33–43. [CrossRef]
10. Thienert, C.; Pulsfort, M. Segment design under consideration of the material used to fill the annular gap. *Geomech. Tunn.* **2011**, *4*, 665–679. [CrossRef]
11. Do, N.A.; Dias, D.; Oreste, P.; Djeran-Maigre, I. 2D numerical investigation of segmental tunnel lining behaviour. *Tunn. Undergr. Space Technol.* **2013**, *37*, 115–127. [CrossRef]
12. Chaiyaput, S.; Sugimoto, M. Effect of boundary conditions in segmental lining model on its sectional force. *Lowl. Technol. Int.* **2016**, *18*, 9–22. [CrossRef]
13. Vitali, O.P.M.; Celestino, T.B.; Bobet, A. 3D finite element modelling optimization for deep tunnels with material nonlinearity. *Undergr. Space* **2018**, *3*, 125–139. [CrossRef]
14. Nematollahi, M.; Dias, D. Three-dimensional numerical simulation of pile-twin tunnels interaction-Case of the Shiraz subway line. *Tunn. Undergr. Space Technol.* **2019**, *86*, 75–88. [CrossRef]
15. RTRI (Railway Technical Research Institute). *Design Standards for Railway Structures and Commentary (Shield Tunnel)*; Maruzen: Tokyo, Japan, 1997; p. 60. (In Japanese)
16. AFTES (French Tunnelling and Underground Space Association). *Recommendation for the Design, Sizing and Construction of Precast Concrete Segments Installed at the Rear of a Tunnel Boring Machine (TBM)*; AFTES: Paris, France, 2005; p. 232.
17. ITA (International Tunnelling Association). Guidelines for the design of shield tunnel lining. *Tunn. Undergr. Space Technol.* **2000**, *15*, 303–331. [CrossRef]
18. BTS (British Tunnelling Society). *Tunnel Lining Design Guide*; Thomas Telford Ltd.: London, UK, 2004.
19. AASHTO (American Association of State Highway and Transportation Officials). *Technical Manual for Design and Construction of Road Tunnels—Civil Elements*; AASHTO: Washington, DC, USA, 2010; pp. 10–14.
20. DAUB (Deutscher Ausschuss fur Unterirdisches Bauen). *Recommendations for the Design, Production and Installation of Segmental Rings*; Technical Report Deutscher Ausschuss fur unterirdisches Bauen e.V; DAUB: Cologne, Germany, 2013; p. 23.
21. JSCE (Japan Society of Civil Engineers). *Standard Specifications for Tunneling–2016: Shield Tunnels*; Japan Society of Civil Engineers: Tokyo, Janpan, 2016.
22. OVBB (Austrian Association for Concrete and Construction Technology). *Guideline Concrete Segmental Lining Systems*; OVBB: Apeldoorn, The Netherlands, 2011; p. 18.

23. Koyama, Y.; Nishimura, T. The design of lining segment of shield tunnel using a spring model with two ring beams. *Proc. Tunn. Eng. JSCE* **1997**, *7*, 279–284. (In Japanese)
24. Do, N.A.; Dias, D.; Oreste, P.; Djeran-Maigre, I. A new numerical approach to the hyperstatic reaction method for segmental tunnel linings. *Int. J. Numer. Anal. Methods Geomech.* **2014**, *38*, 1617–1632. [CrossRef]
25. Vu, M.N.; Broere, W.; Bosch, J.W. Structural analysis for shallow tunnels in soft soils. *Int. J. Geomech.* **2017**, *17*. [CrossRef]
26. Mashimo, H. Ishimura, T. In Numerical modelling of the behavior of shield tunnel lining during assembly of a tunnel ring. In Proceedings of the 5th International Symposium TC28 on Geotechnical Aspects of Underground Construction in Soft Ground, Taylor & Francis, Amsterdam, The Netherlands, 15–17 June 2005; pp. 587–593.
27. Kimura, S.; Kanda, H.; Nanmoku, T.; Koizumi, A. Applicability of the beam-spring model with ground springs set all around the lining to design of shield tunnel lining by comparison of in-situ measurements and the sensitivity analysis. *J. Jpn. Soc. Civ. Eng.* **2002**, *721*, 119–138. (In Japanese)
28. Sugimoto, M.; Chen, J.; Sramoon, A. Frame structure analysis model of tunnel lining using nonlinear ground reaction curve. *Tunn. Undergr. Space Technol.* **2019**, *94*, 1–7. [CrossRef]
29. Duddeck, H. Empfehlungen zur Berechnung von Tunneln im Lockergestein. *Die Bautech.* **1980**, *57*, 349–356. (In German)
30. Arnau, O.; Molins, C. Experimental and analytical study of the structural response of segmental tunnel linings based on an in situ loading test. Part 2: Numerical simulation. *Tunn. Undergr. Space Technol.* **2011**, *26*, 778–788. [CrossRef]
31. Sramoon, A.; Sugimoto, M. Development of ground reaction curve for shield tunnelling. In *Geotechnical Aspects of Underground Construction in Soft Ground*; Balkema: Rotterdam, The Netherlands, 2000; pp. 431–436.
32. Plizzari, G.A.; Tiberti, G. Steel fibers as reinforcement for precast tunnel segments. *Tunn. Undergr. Space Technol.* **2006**, *21*, 438–439. [CrossRef]
33. Molins, C.; Arnau, O. Experimental and analytical study of the structural response of segmental tunnel linings based on an in situ loading test. Part 1: Test configuration and execution. *Tunn. Undergr. Space Technol.* **2011**, *26*, 764–777. [CrossRef]
34. Itasca Consulting Group, Inc. *Fast Lagrangian Analysis of Continua, User's Guide, Version 5.1*; Itasca Consulting Group, Inc: Minneapolis, MN, USA, 2016.
35. ACTEC (Advanced Construction Technology Center). *Manual on Structural Design of Segmental Lining with the Consideration of Inner Water Pressure*; ACTEC: Tokyo, Japan, 1999; p. 86. (In Japanese)
36. Sugimoto, M.; Sramoon, A. Theoretical model of shield behavior during excavation: I. Theory. *J. Geotech. Environ. Eng.* **2002**, *128*, 138–155. [CrossRef]
37. DIANA FEA BV. *Finite Element Analysis, User's Manual*; Release 10.3; DIANA FEA BV: Delft, The Netherlands, 2019.